Original Article

Fracture mapping of complex intra-articular calcaneal fractures

Ming Ni[1#], Miko Lin Lv[2#], Wanju Sun[1], Yingqi Zhang[3], Jiong Mei[4], Duo Wai-Chi Wong[5,6], Haowei Zhang[2], Yongwei Jia[7], Ming Zhang[5,6]

[1]Department of Orthopaedics, Pudong New Area People's Hospital Affiliated to Shanghai University of Medicine and Health Sciences, Shanghai, China; [2]School of Medical Instrument and Food Engineering, University of Shanghai for Science and Technology, Shanghai, China; [3]Department of Orthopaedics, Tongji Hospital of Tongji University, Shanghai, China; [4]Department of Orthopaedics, Shanghai Sixth People's Hospital Affiliated to Shanghai Jiao Tong University, Shanghai, China; [5]Department of Biomedical Engineering, The Hong Kong Polytechnic University, Hong Kong, China; [6]The Hong Kong Polytechnic University Shenzhen Research Institute, Shenzhen, China; [7]Department of Spine Surgery, Guanghua Hospital Affiliated to Shanghai University of Traditional Chinese Medicine, Shanghai, China

Contributions: (I) Conception and design: M Ni, ML Lv; (II) Administrative support: M Ni, Y Jia, M Zhang; (III) Provision of study materials or patients: M Ni, W Sun, J Mei, Y Jia; (IV) Collection and assembly of data: M Ni, ML Lv; (V) Data analysis and interpretation: M Ni, ML Lv, DW Wong; (VI) Manuscript writing: All authors; (VII) Final approval of manuscript: All authors.

[#]These authors contributed equally to this work.

Correspondence to: Yongwei Jia. Department of Spine Surgery, Guanghua Hospital Affiliated to Shanghai University of Traditional Chinese Medicine, Shanghai 200052, China. Email: spinejia@163.com.

Background: Intra-articular calcaneal fracture remains challenging to manage. Computed tomography and fracture mapping are useful for the diagnosis and treatment of calcaneal fractures. The aim of the present study was to characterize calcaneal fracture patterns using fracture mapping.

Methods: Sixty-two calcaneal fractures were retrospectively included in the study. For each case, the fracture was simulated reduction manually. The fracture lines and zones of comminution were graphically superimposed onto an intact calcaneal template to identify fracture patterns. Major fracture lines and comminution were assessed by focusing on the posterior joint facet, medial wall, lateral wall, sustentaculum tali, and anterior process.

Results: The fracture lines were mostly concentrated on the area anterior to the posterior joint facet and extended medially. The longitudinal lines ran posteriorly from the angle of Gissane, and separated the sustentaculum tali and medial wall from the calcaneal tuberosity. In the lateral wall, the fracture lines extended posteriorly with some branches to the bottom of the calcaneus. No fracture lines passed through the sustentaculum tali. Fracture lines of the posterior tuberosity and anterior process were rare.

Conclusions: Calcaneal fracture lines follow characteristic patterns, which are closely related to the bone structure and fracture mechanism. These fracture patterns will aid clinicians choose surgical approach and fixations in the treatment of calcaneal fractures.

Keywords: Calcaneal fracture; fracture pattern; mapping; 3D computed tomography; classification

Submitted Nov 09, 2020. Accepted for publication Dec 23, 2020.
doi: 10.21037/atm-20-7824
View this article at: http://dx.doi.org/10.21037/atm-20-7824

Introduction

Calcaneal fractures represent approximately 1–2% of all fractures and 65% of tarsal fractures. Approximately 75% of calcaneal fractures are intra-articular fractures (1). The majority of calcaneal fractures are due to a high-energy injury mechanism and occur in young, active working-age men (26–45 years) (2). Anatomic reduction and stable fixation are the accepted treatments for these injuries. However, the treatment of calcaneal fractures remains a challenge due to the complex fracture patterns and high rates of complications, including wound infection,

osteomyelitis and posttraumatic arthritis.

Understanding calcaneal fracture patterns is of great importance for proper management. Essex-Lopresti first described calcaneal fracture patterns and divided them into two major categories, intra-articular and extra-articular, based on plain radiography (3). Sanders *et al.* proposed a classification to describe the number and position of fracture lines that enter the posterior facet according to coronary computed tomography (CT) images (4). However, none of these classifications address the 3D morphologies of calcaneal fractures.

With the development of 3D CT and medical image processing software, a novel method, fracture mapping, was developed to describe the distribution of fracture lines. Fracture mapping can record the size, shapes, numbers, and orientations of fracture fragments, and help surgeons determine the optimal treatment (5). To date, fracture mapping has been applied to scapular, tibial, hip, and acetabular fractures (6-11). However, there have been no reports concerning fracture mapping for the treatment of calcaneal fractures.

The aim of the present study was to identify the location and distribution of fractures of the calcaneus by fracture mapping. We hypothesized that mapping would reveal more detailed patterns of fragments and fracture lines than previous X-ray and CT reports. Based on mapping, the injury mechanism, calcaneal structure, surgical approach and fixations could be evaluated carefully.

We present the following article in accordance with the MDAR reporting checklist (available at http://dx.doi.org/10.21037/atm-20-7824).

Methods

Eligibility criteria

The present study conformed to the provisions of the Declaration of Helsinki (as revised in 2013) and was approved by the Ethics Committee of Shanghai Pudong New Area People's Hospital (No. 2019-16). Cases of calcaneal fractures between September 2015 and May 2019 were retrospectively reviewed. Their consent for this retrospective analysis was waived. The inclusion criteria were as follows: (I) intra-articular calcaneal fracture; (II) patient age ≥18 years; and (III) preoperative CT slice thickness <1.5 mm. The exclusion criteria were as follows: (I) associated foot and ankle fractures; (II) open fractures; and (III) pathological fractures.

Fracture models

All patients underwent CT scans (Siemens, Berlin, Germany) with 1-mm slice interval and 0.5-mm pixel size, and the images were preserved as Digital Imaging and Communications in Medicine (DICOM) files. The DICOM files were then imported into Mimics 15.0 (Materialise, Leuven, Belgium) for model reconstruction. Mimics is a professional software for the analysis of medical images. In Mimics, the fractures were virtually reduced by the function of movement and rotation (*Figure 1*).

Calcaneal templates

Next, 3-matic software (Materialise, Belgium) was used to export the 3D calcaneal model. The calcaneus model was observed in five views—superior, medial, lateral, anterior, and posterior—to analyze the fracture lines.

Fracture mapping

The fracture mapping technique was adopted from Yao *et al.* and Cole *et al.* (10,12). The reduced calcaneal fracture models were imported into 3-matic software and adjusted to best match the 3D calcaneal templates. With transparent processing, the fracture lines were clearly observed and delineated on the template (*Figure 1*). All fracture lines were graphically superimposed, and the fracture map was built (*Figure 2*). To obtain a better understanding of the fracture distribution, the superimposed fracture map was exported to E-3D software (Central South University, Changsha, China) and transformed into 3D heat maps (*Figure 3*). On the 3D heat maps, the relative frequency of the fracture lines is shown by different colors (blue to red, indicating low to high incidence).

Data analysis

The analysis of the fracture maps was descriptive. Patient characteristics were summarized as the mean and standard deviation for continuous variables, and percentage for categorical variables.

Results

Patient characteristics

The final cohort included 62 patients with an average age of 46.2 years (range, 20–58 years). Forty-seven patients

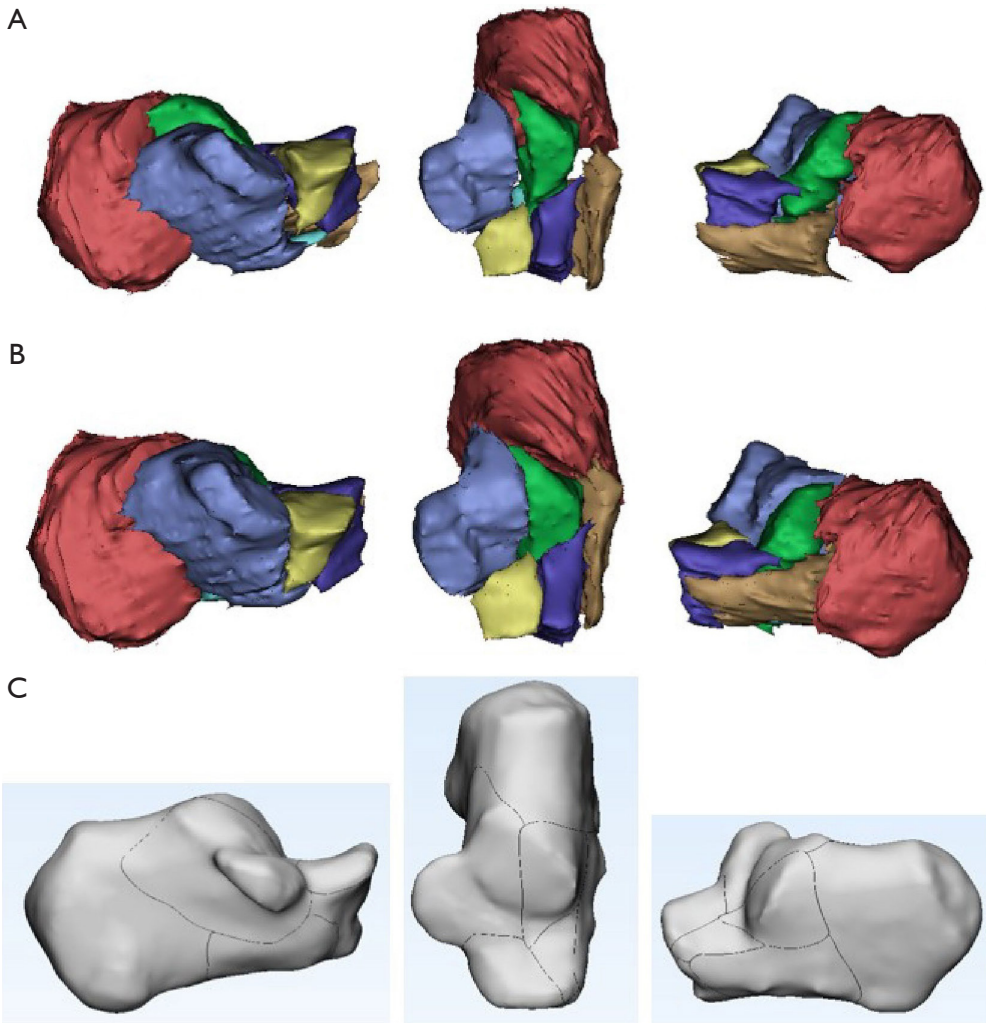

Figure 1 Fracture mapping process. Every fragment was reconstructed in Mimics (A). Fracture fragments were virtually reduced in the 3D views (B). Fracture lines were transcribed onto the 2-dimensional template in 3-matic software (C).

were male, and 15 were female. In total, 38 right and 24 left feet were affected (*Table 1*). There were 15 type II, 16 type III, and 31 type IV fractures according to the Sanders classification. Of the fractures, 52 were caused by falls from height, and 10 were caused by motor accidents.

Fracture maps

The fracture maps are shown in *Figure 4*. From the superior view, the major fracture lines were mostly concentrated in the area anterior to the posterior joint facet and extended in the transverse and longitudinal directions (*Figure 4A*). The transverse lines ran inward through the calcaneus sulcus and reached the medial wall slightly anterior to the middle facet joint. These lines also extended anteriorly to involve the calcaneocuboid joint. The longitudinal fracture lines started from the calcaneus sulcus, passed through the middle part of the posterior facet, extended posteromedially, and split the calcaneus into anteromedial and posterolateral fragments.

In the medial wall, the fracture lines mostly ran through the middle of the calcaneal tuberosity and continued with the upper longitudinal lines and anterior transverse lines (*Figure 4B*). In the lateral wall, the fracture lines started from the critical angle of Gissane and extended posteriorly to the rear of the tuberosity, with some branches running to the bottom of the calcaneus (*Figure 4C*).

No fracture lines passed through the sustentaculum tali. Fracture lines of the posterior, superior, and

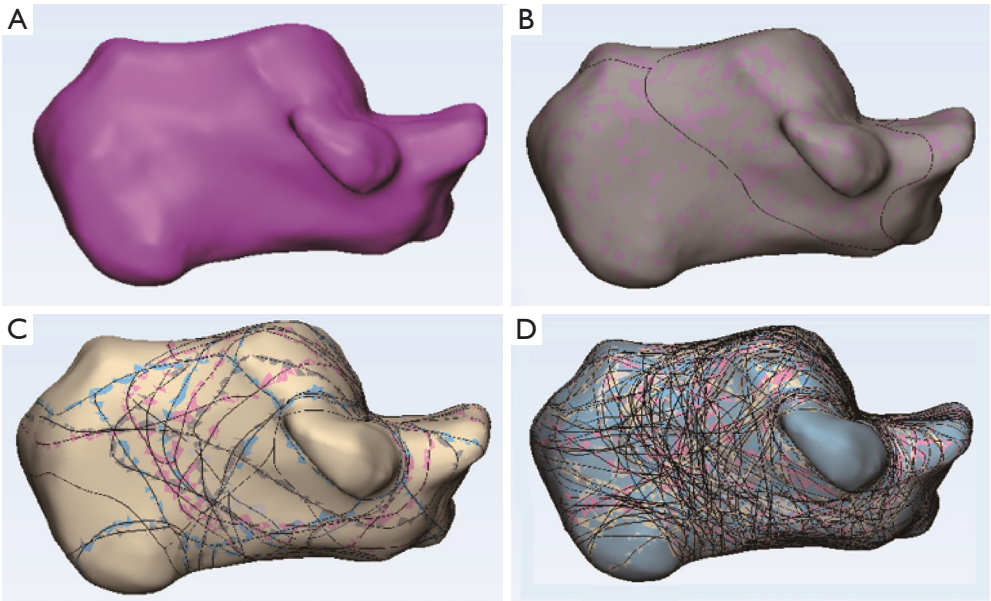

Figure 2 Method used for 3D computed tomography mapping of calcaneal fractures. Intact calcaneal template (A), fracture model marked with a line (B), model with 20 superimposed lines (C), and model of all 62 fracture lines (D).

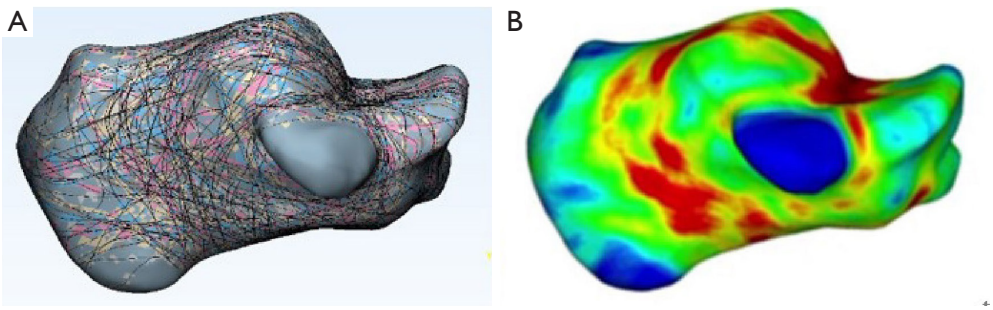

Figure 3 Comparison of calcaneal fracture lines: fracture map (A) and heat map (B). The density of fracture lines in heat map is shown by different colors (blue to red, indicating low to high incidence).

inferior parts of the calcaneal tuberosity were rare. In the calcaneocuboid joint (CCJ) facet, the fracture lines passed through the medial one-third aspect of the articular surface (*Figure 4D*).

Discussion

To the best of our knowledge, the present study was the first to analyze calcaneal fracture patterns with fracture mapping technology. The principal finding was that the calcaneal fracture lines were mostly concentrated along the calcaneus sulcus, and extended medially, posteriorly, and anteriorly to affect the posterior facet and cortical walls. This result revealed the weak structures inside the calcaneus, and provided more detailed information than previous anatomy and radiology reports. It also help clinicians choose the most suitable surgical approaches and fixations for calcaneal fractures.

At present, the most commonly used calcaneal fracture classifications include the Essex-Lopresti classification and Sanders classification. Essex-Lopresti divided calcaneal fractures into two categories based on X-ray: tongue type fracture and joint depression fracture. The difference between the two types is the connection of the calcaneal tuberosity to the lateral portion of the posterior facet, which is present in the tongue type and absent in the

Table 1 Patient demographics

Demographic	Data (n=62)
Mean age, years (SD)	
Male	46.2 (13.4)
Female	38.4 (11.5)
Total	42.5 (12.7)
Sex, n (%)	
Male	47 (75.8)
Female	15 (24.2)
Foot, n (%)	
Left	24 (38.7)
Right	38 (61.3)
Sanders classification, n (%)	
II	15 (24.2)
III	16 (25.8)
IV	31 (50.0)
Fracture mechanism, n (%)	
Fall from height	52 (83.9)
Motor accident	10 (16.1)

SD, standard deviation.

joint depression type (3). Sanders *et al.* proposed that intra-articular calcaneal fractures can be divided into type II (2 fragments of the posterior joint facet), type III (3 fragments), and type IV (>3 fragments), according to coronary CT images. However, both of these classifications have certain limitations in the description of injuries (4). The Essex-Lopresti classification cannot reflect the involvement of the subtalar joint facets and medial wall. In the Sanders classification, the pathological changes of calcaneal fractures are not described. Therefore, a novel classification that can reflect morphological changes and the subtalar joint facets should be proposed to guide clinical treatment.

Several studies have described the position and direction of calcaneal fracture lines (13-15). Essex-Lopresti believed that the anterolateral process of the talus produced a primary fracture line beginning at the angle of Gissane, and extended medially to split the middle facet and superomedial fragment (3). Teubner *et al.* found that, when the foot is in plantar flexion during impact, a tongue-type fracture occurs, and when the foot is in dorsiflexion, a joint depression fracture occurs (16). Warrick and Bremner found that the primary fracture lines extend from the medial side behind the sustentaculum tali forward and laterally for variable distances (17). Tsubone *et al.* predicted

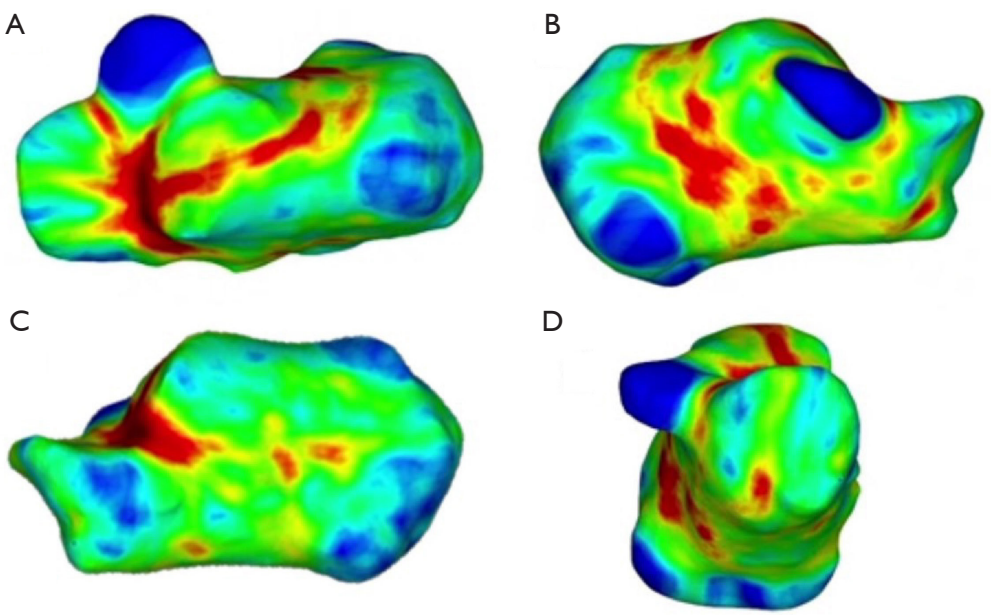

Figure 4 Heat map of calcaneal fracture lines: superior (A), medial (B), lateral (C), and anterior views (D).

the calcaneus fracture lines using the finite element (FE) model (18). Their results showed that the fracture lines always started at the lateral side of the posterior articular fragment and extended along the anteromedial and anterolateral directions (18). In the present study, we found that the fracture lines were distributed regularly along the calcaneal surface. The major transverse fracture line was located anterior to the posterior facet joint and extended along the calcaneus sulcus. The longitudinal fracture lines originated from the transverse lines, extended posteriorly, and separated the posterior facet and medial wall from the tuberosity. In the lateral wall, the fracture lines extended horizontally to the rear of the calcaneal tubercle. These findings provide a good basis for the choice of surgical incision and fixation methods.

The calcaneal fracture line distribution correlated well with the internal architecture and biomechanics of the calcaneus. The calcaneus is the largest tarsal bone, with a thin cortical shell enclosing cancellous bones (19). Athavale *et al.* sectioned 50 adult human calcanei in various planes to study the internal architecture (20). Their results showed that the cortical shell was weak on the anterior border of the posterior subtalar facet in the coronal plane. Inside the calcaneus, the trabecular system was regularly arranged, but there was a triangle-shaped area of sparse or absent trabeculae in the antero-inferior part of the calcaneus (20). This position was consistent with the major fracture lines in the heat map. In another study, Wong *et al.* analyzed the influence of foot impact on the risk and positions of calcaneus fracture by FE analysis (21). The prediction showed that an axial compressive impact could produce considerable yielding of trabecular bone in the calcaneus, predisposing the calcaneus to the risk of fracture. The von Mises and Tresca stresses were mostly concentrated at the angle of Gissane and posterior facet joint. This was also in agreement with our findings.

The sustentaculum tali is rarely involved in calcaneal fractures, and provides an effective site for screw fixation (22). Della Rocca evaluated more than 300 patients with calcaneal fractures and found only 19 isolated sustentacular fractures (23). Another study showed that solitary fractures of the sustentaculum tali without additional calcaneal injuries occur in less than 1% of all calcaneal fractures (24). In the present study, we found that no fracture lines passed from the sustentaculum tali. In addition, the fracture lines ran from the superomedial to inferolateral direction in the coronary plane. This can be attributed to the unique position between the talus and calcaneus. The center of the calcaneus tuberosity was slightly lateral to the center of the talus (25). This relation will produce an eccentric shear force through the calcaneal body and break the calcaneus along the stress line. This indicates that, when applying screw fixation from the lateral side, the direction should be obliquely upward to pass through the fracture perpendicularly.

Lateral wall rupture is a typical characteristic of calcaneal fractures. The fracture line typically appears as an inverted "Y" pattern, with the posterior limb extending horizontally as a tongue-type fracture or vertically as a joint depression-type fracture (26). In the present study, we found that the fracture lines of the lateral wall were always oriented from the critical angle of Gissane, and extended posteriorly to the calcaneal tuberosity. This was similar to previous reports. However, the vertical fracture line is relatively uncommon. Observing the fracture lines can help surgeons choose appropriate surgical approaches. The sinus approach was the most commonly used minimally invasive approach for calcaneal fractures. However, its position was slightly higher than the lateral fracture lines. This indicates that a lower approach might be more beneficial for fracture exposure and reduction.

In the present study, we showed that fracture line distribution in the anterior process of the calcaneus was rare, but the CCJ facet was involved with the fracture lines. The reported incidence of CCJ involvement in calcaneal fractures varies from 33% to 76% (27). Previous studies have suggested that unsatisfactory reduction of the CCJ might lead to impingement symptoms or lateral peritalar subluxation (28). Therefore, surgeons should be cautious about the management of calcaneal fractures extending into the CCJ in their operative steps. In the fracture maps, the lines were located on the medial one-third aspect of the CCJ surface. This might not be obvious on X-rays, and CT scanning should be routinely performed.

The present study has some limitations. First, the number of patients in the study was relatively small. However, all types of intra-articular calcaneal fractures were included and this group could stood for calcaneal fractures to some extent. A larger number of cases may lead to more accurate results. Second, the methods and results were qualitative rather than quantitative, and fracture line distributions of different types of calcaneal fractures were not compared. Third, because of the anatomical variability of the calcaneus, some fracture images did not perfectly match the 3D calcaneal model. Therefore, the fracture lines drawn on the calcaneus model might be slightly different

from true fracture patterns.

Conclusions

In conclusion, this study describes the morphologic characteristics of calcaneal fractures from multiple perspectives. The principal findings of this study are as follows:

(I) There are characteristic patterns of calcaneal fractures, which are closely related to the calcaneal structure and fracture mechanism.
(II) There is a high incidence of fracture lines in the anterior border of the posterior facet joint.
(III) Fractures frequently split the posterior facet joint, extending posteriorly to separate the anteromedial fragment from the calcaneal tuberosity.
(IV) Fractures rarely involve the sustentaculum tali, posterior calcaneal tuberosity and anterior process.

These results will help physicians consider treatments for calcaneal fractures, including surgical approaches, preoperative planning, implant choice and fixation strategies.

Acknowledgments

Funding: This research was funded by the Project of Novel Interdisciplinary of Health System in Pudong New Area, Shanghai, grant number PWXx2020-08, General Project of Shanghai Municipal Health Bureau, grant number 201840137 & 201840361, Key R&D Program from the Ministry of Science and Technology of China, grant number 2018YFB1107000, General Program from the National Natural Science Foundation of China, grant number 11972315, Key Program from the National Natural Science Foundation of China, grant number 11732015.

Footnote

Reporting Checklist: The authors have completed the MDAR reporting checklist. Available at http://dx.doi.org/10.21037/atm-20-7824

Data Sharing Statement: Available at http://dx.doi.org/10.21037/atm-20-7824

Conflicts of Interest: All authors have completed the ICMJE uniform disclosure form (available at http://dx.doi.org/10.21037/atm-20-7824).The authors have no conflicts of interest to declare.

Ethical Statement: The authors are accountable for all aspects of the work in ensuring that questions related to the accuracy or integrity of any part of the work are appropriately investigated and resolved. The present study conformed to the provisions of the Declaration of Helsinki (as revised in 2013) and was approved by the Ethics Committee of Shanghai Pudong New Area People's Hospital (No. 2019-16). Informed consent for this retrospective analysis was waived.

References

1. Marouby S, Cellier N, Mares O, et al. Percutaneous arthroscopic calcaneal osteosynthesis for displaced intra-articular calcaneal fractures: Systematic review and surgical technique. Foot Ankle Surg 2020;26:503-8.
2. Alexandridis G, Gunning AC, Leenen LPH. Health-related quality of life in trauma patients who sustained a calcaneal fracture. Injury 2016;47:1586-91.
3. Essex-Lopresti P. The mechanism, reduction technique, and results in fractures of the os calcis. Br J Surg 1952;39:395-419.
4. Sanders R, Fortin P, DiPasquale T, et al. Operative treatment in 120 displaced intraarticular calcaneal fractures: results using a prognostic computed tomography scan classification. Clin Orthop Relat Res 1993;290:87-95.
5. Dugarte AJ, Tkany L, Schroder LK, et al. Comparison of 2 vs 3 dimensional fracture mapping strategies for 3 dimensional computerized tomography reconstructions of scapula neck & body fractures. J Orthop Res 2018;36:265-71.
6. Yang Y, Zou C, Fang Y. A study on fracture lines of the quadrilateral plate based on fracture mapping. J Orthop Surg Res 2019;14:310.
7. McGonagle L, Cordier T, Link B, et al. Tibia plateau fracture mapping and its influence on fracture fixation. J

Orthop Traumatol 2019;20:12.
8. Mellema JJ, Eygendaal D, van Dijk CN, et al. Fracture mapping of displaced partial articular fractures of the radial head. J Shoulder Elbow Surg 2016;25:1509-16.
9. Molenaars RJ, Mellema JJ, Doornberg JN, et al. Tibial plateau fracture characteristics: computed tomography mapping of lateral, medial, and bicondylar fractures. J Bone Joint surg Am 2015;97:1512-20.
10. Yao X, Zhou K, Lv B, et al. 3D mapping and classification of tibial plateau fractures. Bone Joint Res 2020;9:258-67.
11. Li M, Li ZR, Li JT, et al. Three-dimensional mapping of intertrochanteric fracture lines. Chin Med J (Engl) 2019;132:2524-33.
12. Cole PA, Mehrle RK, Bhandari M, et al. The pilon map: Fracture lines and comminution zones in OTA/AO Type 43C3 pilon fractures. J Orthop Trauma 2013;27:e152-6.
13. Carr JB. Mechanism and pathoanatomy of the intraarticular calcaneal fracture. Clin Orthop Relat Res 1993;290:36-40.
14. Burdeaux BD. Reduction of calcaneal fractures by the mcReynolds medial approach technique and its experimental basis. Clin Orthop Relat Res 1983;177:87-103.
15. Daqiq O, Sanders F, Schepers T. How does mechanism of injury relate to similar fracture patterns in bilateral displaced intra-articular calcaneal fractures? J Foot Ankle Surg 2020;59:1162-6.
16. Teubner E, Gerstenberger F, Walter B. Pathomechanical aspects of intra-articular calcaneus fractures. Typing, grading and surgical therapy. Aktuelle Traumatol 1992;22:243-50.
17. Warrick CK, Bremner AE. Fractures of the calcaneum, with an atlas illustrating the various types of fracture. J Bone Joint Surg Br 1953;35-B:33-45.
18. Tsubone T, Toba N, Tomoki U, et al. Prediction of fracture lines of the calcaneus using a three-dimensional finite element model. J Orthop Res 2019;37:483-9.
19. Sabry FF, Ebraheim NA, Mehalik JN, et al. Internal architecture of the calcaneus: implications for calcaneus fractures. Foot Ankle Int 2000;21:114-8.
20. Athavale SA, Joshi SD, Joshi SS. Internal architecture of calcaneus: correlations with mechanics and pathoanatomy of calcaneal fractures. Surg Radiol Anat 2010;32:115-22.
21. Wong DW, Niu W, Wang Y, et al. Finite element analysis of foot and ankle impact injury: risk evaluation of calcaneus and talus fracture. PLos One 2016;11:e0154435.
22. Della Rocca GJ, Nork SE, Barei DP, et al. Fractures of the sustentaculum tali: injury characteristics and surgical technique for reduction. Foot Ankle Int 2009;30:1037-41.
23. Al-Ashhab ME, Elgazzar AS. Treatment for displaced sustentaculum tali fractures. Foot (Edinb) 2018;35:70-4.
24. Gitajn IL, Abousayed, M, Toussaint RJ, et al. Anatomic alignment and integrity of the sustentaculum tali in intra-articular calcaneal fractures: is the sustentaculum tali truly constant? J Bone Joint Surg Am 2014;96:1000-5.
25. Yoganandan N, Pintar FA, Seipel R. Experimental production of extra- and intra-articular fractures of the os calcis. J Biomech 2000;33:745-9.
26. Lowery RBW, Calhoun JH. Fractures of the calcaneus. Part I: Anatomy, injury mechanism, and classification. Foot Ankle Int 1996;17:230-5.
27. Kinner B, Schieder S, Müller F, et al. Calcaneocuboid joint involvement in calcaneal fractures. J Trauma 2010;68:1192-9.
28. Massen FK, Baumbach SF, Herterich V, et al. Fractures to the anterior process of the calcaneus-clinical results following functional treatment. Injury 2019;50:1781-6.

(English Language Editor: R. Scott)

Cite this article as: Ni M, Lv ML, Sun W, Zhang Y, Mei J, Wong DW, Zhang H, Jia Y, Zhang M. Fracture mapping of complex intra-articular calcaneal fractures. Ann Transl Med 2021;9(4):333. doi: 10.21037/atm-20-7824